Excitation and Control of Plasma Wakefields by Multiple Laser Pulses

J. Cowley,[1] C. Thornton,[1] C. Arran,[1] R. J. Shalloo,[1] L. Corner,[1] G. Cheung,[1] C. D. Gregory,[2] S. P. D. Mangles,[3] N. H. Matlis,[4] D. R. Symes,[2] R. Walczak,[1] and S. M. Hooker[1,*]

[1]*John Adams Institute for Accelerator Science, University of Oxford, Denys Wilkinson Building, Keble Road, Oxford OX1 3RH, United Kingdom*

[2]*Central Laser Facility, Rutherford Appleton Laboratory, Didcot OX11 0QX, United Kingdom*

[3]*John Adams Institute for Accelerator Science, Blackett Laboratory, Imperial College London, London SW7 2AZ, United Kingdom*

[4]*Deutsches Elektronen-Synchrotron (DESY), Notkestraße 85, Hamburg 22607, Germany*

(Received 15 March 2017; revised manuscript received 31 May 2017; published 27 July 2017)

We demonstrate experimentally the resonant excitation of plasma waves by trains of laser pulses. We also take an important first step to achieving an energy recovery plasma accelerator by showing that a plasma wave can be damped by an out-of-resonance trailing laser pulse. The measured laser wakefields are found to be in excellent agreement with analytical and numerical models of wakefield excitation in the linear regime. Our results indicate a promising direction for achieving highly controlled, GeV-scale laser-plasma accelerators operating at multikilohertz repetition rates.

DOI: 10.1103/PhysRevLett.119.044802

Particle accelerators lie at the heart of many areas of science, technology, and medicine either through direct application of the particle beams or by driving radiation sources such as synchrotrons and free-electron lasers (FELs). With conventional radio-frequency (RF) technology the electric field used to accelerate particles is typically less than 100 MV m^{-1}, which is a significant factor determining the size and cost of the machine. In distinct contrast, plasma accelerators can generate gradients of order 100 GV m^{-1}, which shrinks the length of the acceleration stage by orders of magnitude.

In a plasma accelerator the acceleration field is generated within a trailing plasma wakefield excited by displacement of the plasma electrons by a driving laser pulse [1–4] or particle bunch [5,6]. Laser-driven plasma accelerators have made impressive progress [7] in recent years. They can now generate electron beams with energies comparable to those used in synchrotrons and FELs (a few GeV), but in accelerator stages only a few centimetres long [8–10], with bunch durations in the femtosecond range [11–13], and with properties ideal for generating femtosecond duration visible to x-ray pulses [14–20].

In almost all recent work the plasma wakefield has been driven by single laser pulses from high-power Ti:sapphire chirped-pulse-amplification laser systems. Unfortunately, these have very low wall-plug efficiency (<0.1%) and cannot readily operate at pulse repetition frequencies much above $f_{\mathrm{rep}} = 10$ Hz. At present, therefore, the driver parameters severely restrict the number of potential applications of laser-plasma accelerators.

We recently reexamined [21] multipulse laser wakefield acceleration (MP-LWFA) in which the wakefield is excited by a train of low-energy laser pulses, rather than by a single, high-energy pulse. If the pulses are spaced by the plasma wavelength $\lambda_{p0} = 2\pi c/\omega_{p0}$, then the wakefields driven by the pulses in the train add coherently, causing the plasma wave amplitude to grow towards the back of the train. Here, the plasma frequency is $\omega_{p0} = 2\pi/T_{p0} = (n_{e0}e^2/m_e\epsilon_0)^{1/2}$, where n_{e0} is the ambient electron density. We note that Benedetti *et al.* [22] have studied an alternative scheme in which the wakefield is driven by an incoherent combination of laser pulses arranged longitudinally, or transversely, within a single plasma period.

Using a train of low-energy laser pulses opens plasma accelerators to novel laser technologies, such as fiber or thin-disk lasers, which cannot directly deliver joule-level short pulses, but which can provide lower-energy pulses with f_{rep} in the kilohertz range, whilst achieving wall-plug efficiencies at least 2 orders of magnitude higher than conventional solid-state lasers [23]. Our recent analysis [21] showed that a MP-LWFA driven by a near-term laser system of this type could drive wakefields with an accelerating field of 4.7 GV m^{-1}, with a dephasing-limited energy gain of 0.75 GeV, and that with $f_{\mathrm{rep}} = 10$ kHz these could drive compact coherent and incoherent x-ray sources with average brightnesses exceeding those available from large scale, nonsuperconducting, RF accelerators. A further advantage of MP-LWFA is that it provides a natural architecture for "energy recovery": the use of one or more trailing laser pulses to remove (and potentially recycle) energy remaining in the wakefield after particle acceleration. Energy recovery is likely to be an important capability in future plasma accelerators operating at high average powers.

In this Letter we present the first demonstration of wakefield excitation by a laser pulse structure that is long compared to the plasma period, and for which there is

sufficient control of the temporal profile to overcome relativistic saturation. We also take an important first step towards achieving energy recovery by showing that a suitably delayed laser pulse can damp the plasma wave driven by a leading pulse. We achieve this through measurements of plasma waves by frequency domain holography (FDH) and a new analysis method, temporally encoded spectral shifting (TESS) [24]; we demonstrate that these two analyses are in excellent agreement, and that our results are well described by a linear response model of wakefield excitation.

Since laser systems generating directly the pulse trains required for MP-LWFA are still under development, this first demonstration employed a Ti:sapphire laser—the Gemini (Astra TA2) laser at the Rutherford Appleton Laboratory—reconfigured to generate trains of laser pulses. In its standard arrangement this laser delivers to target approximately 600 mJ, 40 fs laser pulses with a center wavelength $\lambda_0 = 800$ nm at $f_{\mathrm{rep}} = 5$ Hz.

Figure 1 shows schematically the experimental arrangement employed (see Supplemental Material [25] for further details of the experimental arrangement and analysis methods). Single, temporally chirped pulses from the laser system were converted into pulse trains by placing a Michelson interferometer between the final laser amplifier and its vacuum compressor, as discussed in Refs. [26,27]. The Michelson acted as a spectral filter with a spectral intensity transmission of the form $T(\omega) = \cos^2(\omega\Delta x/2c)$, where Δx is the path difference between the Michelson arms. With the compressor set for partial compression, the modulated spectrum transmitted by the Michelson was partially compressed to a train of pulses, with a temporal spacing that could be controlled by adjusting the Michelson and compressor. With the compressor set to give full compression of an unmodulated input pulse, the output of the combination comprised a pair of short (approximately 50 fs) pulses temporally separated by $\delta\tau = \Delta x/c$. The temporal intensity profiles of the pulse trains were

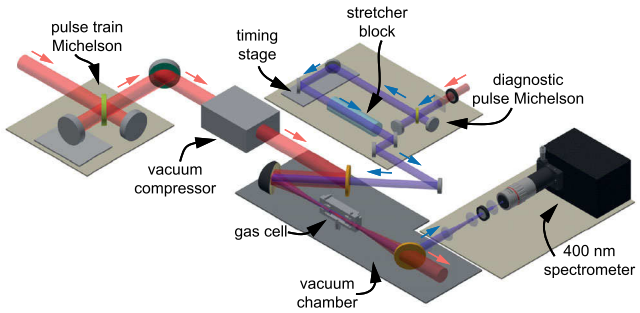

FIG. 1. Schematic diagram of the experiment layout. The propagation path of the driving pulse train is shown in red, and that of the probe and reference beams is shown in blue. The laser compressor and the components shown above the darker base are located in the vacuum chamber; all other components are mounted in air.

determined by combining a model of the laser compressor and pulse train Michelson with measurements of the pulse train spectrum and single-shot autocorrelation (SSA) [27].

The pulse train was directed to an $f = 1$ m off-axis paraboloid, used at $f/18$, which focused the pulses through a hydrogen gas cell; this was 3 mm long, with entrance and exit pinholes of 250 μm diameter. The spot size ($1/e^2$ radius of the transverse intensity profile) of the focused pulse trains was measured to be $w_0 = (35 \pm 5)$ μm.

Plasma wakefields driven by the pulse train were probed by frequency domain holography [28]. In this method a frequency-chirped probe pulse copropagates with the plasma wave and a reference pulse located ahead of the plasma wave. These diagnostic pulses are then interfered in a spectrograph to give a spectral interferogram, with spatial information in the nondispersed direction. When the chirped probe pulse interacts with a plasma wave, each of its frequency components experiences a phase shift that depends on the local wakefield amplitude; after a length ℓ of plasma this phase shift can be written as $\phi_p(\zeta) = (\omega_0/c)\ell[\eta(\zeta) - \eta_0]$, where ω_0 is the angular frequency of the probe pulse, $\zeta = t - \ell/c$, $\eta(\zeta)$ is the refractive index of the plasma, and η_0 is the refractive index experienced by the reference pulse. The spectrum of the combined transmitted probe and reference pulses comprises spectral fringes of angular frequency separation $\Delta\omega = 2\pi/\Delta t$, where Δt is the temporal separation of the probe and reference pulses, modulated by a spectral phase $\Delta\psi(\omega)$ that depends on the wakefield (for an example, see Supplemental Material [25]). Frequency domain holography uses well-known Fourier techniques to extract $\Delta\psi(\omega)$ from the interferogram, and hence the temporal phase shift caused by the plasma wave [28].

In this work we also used a TESS analysis [24] of the same data, which is applicable when the plasma wave is sinusoidal. In this approach a Fourier transform of the interferogram yields a sideband at $t = \Delta t$ and a series of satellites at $t = \Delta t + m\psi^{(2)}\omega_{p0}$ where $m = \pm 1, \pm 2, \pm 3, \ldots$ and $\psi^{(2)}$ is the group delay dispersion (GDD) of the probe and reference pulses. The ratio of the amplitudes of the satellites to the sideband can be shown to be [29]

$$r_m = \frac{J_m(\Delta\phi_p)}{J_0(\Delta\phi_p)}\frac{\mathcal{F}(m\omega_{p0})}{\mathcal{F}(0)}, \tag{1}$$

where $\Delta\phi_p = (\omega_{p0}^2/2\omega_0)(\ell/c)(\delta n_{e0}/n_{e0})$ is proportional to the wake amplitude and

$$\mathcal{F}(m\omega_{p0}) = \int_0^\infty \sqrt{S_{\mathrm{pr,inc}}(\omega + m\omega_{p0})}\sqrt{S_{\mathrm{ref,inc}}(\omega)}d\omega, \tag{2}$$

in which $S_{\mathrm{pr,inc}}(\omega)$ and $S_{\mathrm{ref,inc}}(\omega)$ are the spectra of the incident probe and reference pulses.

A pair of $\lambda = 400$ nm diagnostic pulses, with an adjustable temporal separation Δt, were generated by passing a separately compressed and frequency-doubled fraction of the main laser pulse through a Michelson interferometer. These pulses were chirped and stretched to a duration of around 1.5 ps by sending them through a 160 mm long block of BK7 glass. The diagnostic pulses were propagated colinearly with the driving pulse train by directing them through a dichroic mirror; after propagating through the gas cell they were separated from the pulse train by a second dichroic mirror and imaged onto the entrance slit of a spectrograph.

Figure 2 shows the results of FDH and TESS measurements of the wakes driven by a single laser pulse. An example wakefield retrieved by FDH is shown in Fig. 2(a): the wake can be observed clearly, with a transverse extent that is compatible with the focal spot size of the driving laser, and with wave fronts that are only slightly curved, which is consistent with a linear wakefield. The plasma period, read directly from the plot, is found to be $T_{p0} = (90 \pm 5)$ fs, which agrees with the expected value of $T_{p0} = (91 \pm 2)$ fs for this cell pressure.

The wake in Fig. 2(a) can be observed up to $\zeta \approx 2$ ps after the pump pulse, corresponding to approximately

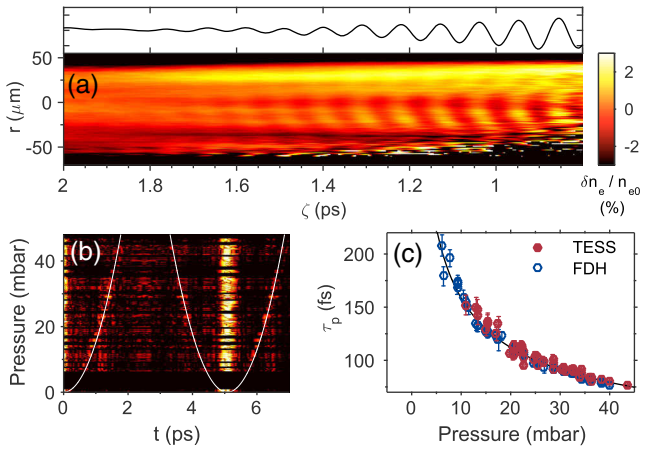

FIG. 2. FDH and TESS analyses of linear plasma wakefields driven by a single laser pulse of energy approximately 270 mJ and pulse duration (46 ± 7) fs. (a) shows an example of the wakefield recovered by FDH for a cell pressure of (31 ± 1) mbar, where $\zeta = 0$ corresponds to the center of the pump pulse. In the panel above, the solid line shows the amplitude of the wakefield averaged over the range $|r| \leq 6$ μm; the ticks on the y axis are at $\delta n_e/n_{e0} = \pm 1\%$. (b) shows a waterfall plot of Fourier transforms of the spectral interferograms, where the magnitude of the Fourier transform is plotted on a logarithmic scale. The solid white line shows the expected position of the satellites calculated from the expected plasma frequency. (c) shows, as a function of the gas pressure, the plasma period determined by the FDH and TESS analyses. The solid curve is the plasma period calculated assuming an electron density equal to twice the density of hydrogen molecules. The error bars are estimated from the uncertainty in determining the satellite separation in (b) and the plasma period in (a).

20 plasma periods. This may be compared with the expected time for the onset of ion motion $T_{p,\mathrm{ion}} = (M/Zm_e)^{1/2} T_{p0} \approx 43 T_{p0}$, where M is the ion mass and $Z = 1$ is the ion charge. For these conditions the characteristic time [30] for momentum transfer by electron-ion collisions is approximately $\tau_{\mathrm{ei}} \approx 48 T_{p0}$. These processes are therefore unlikely to be the sole cause of the apparent decay of the wakefield. An additional reason is the variation of the plasma density along the path of the probe pulse, especially near the entrance and exit pinholes; in this case the number of measurable plasma periods is approximately $n_{e0}/(2\Delta n_{e0})$, where Δn_{e0} is the range of density. The data could therefore be fully explained by a variation $\Delta n_{e0}/n_{e0} \approx 2.5\%$. Further work is necessary to assess the roles of collisions and ion motion; however, we note that our previous particle-in-cell simulations [21] show (for a hydrogen pressure of 3.6 mbar) that linear growth of the wake amplitude with N could be maintained for trains of up to $N = 80$.

Figure 2(b) shows, as a function of the cell pressure, a waterfall plot of Fourier transforms of the spectral interferograms. The sideband at $t = \Delta t \approx 5.1$ ps, corresponding to the probe-reference separation, can be seen clearly, as can the $m = \pm 1$ TESS satellites; the separation of these satellites, and also of a satellite to the DC peak at $t = 0$, follows closely that expected from the measured GDD of the probe pulse and the plasma frequency calculated from the initial gas pressure, assuming full ionization by the driving laser pulse. The plasma periods determined from the FDH and TESS analyses are compared in Fig. 2(c) and are seen to be in excellent agreement with each other and with the calculated plasma period.

Figure 3 shows, as a function of cell pressure, the relative amplitude of the plasma waves driven by trains of $N = 1$, $N = 2$, and $N \approx 7$ pulses, as determined by TESS analyses. In the linear regime the relative amplitude of the plasma wave driven by a single driving pulse with Gaussian transverse and temporal profiles is [31]

$$\frac{\delta n_e}{n_{e0}} = A \omega_{p0} \tau_0 \left[1 + \left(\frac{2\sqrt{2}c}{\omega_{p0} w_0} \right)^2 \right] \exp\left(-\frac{(\omega_{p0}\tau_0)^2}{16 \ln 2} \right), \quad (3)$$

where τ_0 is the full-width at half maximum of the temporal profile, and the parameter A is proportional to the peak laser intensity. Figure 3(a) shows a fit of Eq. (3) to the data, where A and τ_0 are taken as free parameters and ω_{p0} is calculated from the gas pressure. The fit yields $\tau_0 = (49 \pm 8)$ fs, which is consistent with the value of $\tau_0 = (46 \pm 7)$ fs measured with the SSA. Figure 3(a) also shows excellent agreement between the data and a fit to the wakefield amplitude calculated for the measured temporal intensity profile of the driving pulse, the only fitting parameter being the parameter A.

From elementary considerations, in the linear regime the relative amplitude of the wakefield behind a train of N identical driving pulses spaced in time by $\delta\tau$ is

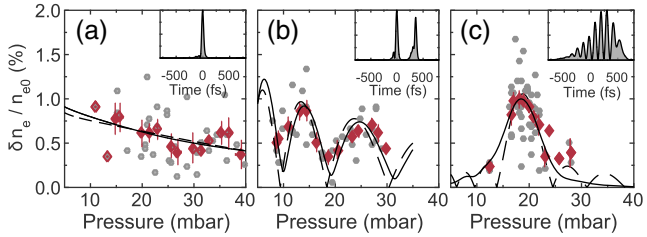

FIG. 3. Relative wakefield amplitudes, as a function of gas cell pressure, measured at delay ζ between the center of the pulse train and the center of the probe pulse for a driving pulse train comprising N pulses of measured pulse separation $\delta\tau$ and total energy E where (a) $N = 1$, $E = 270$ mJ, $\zeta = 2.2$ ps; (b) $N = 2$, $\delta\tau = (420 \pm 20)$ fs, $E = 160$ mJ, $\zeta = 2.5$ ps; and (c) $N \approx 7$, $\delta\tau = (112 \pm 6)$ fs, $E = 170$ mJ, $\zeta = 1.3$ ps. Gray circles show single measurements and red diamonds show the same data averaged over pressure bins of width 4 mbar [(a) and (b)] or 2 mbar (c); the error bars are standard errors and the y axes are the same for all plots. The insets show the measured driving pulse trains. The dashed lines show fits of Eq. (4), and the solid lines show the wake amplitudes calculated for the pulse trains shown in the figure insets.

$$\left(\frac{\delta n_e}{n_{e0}}\right)_N = \left(\frac{\delta n_e}{n_{e0}}\right)_1 \left|\frac{\sin\left(\frac{1}{2}N\omega_{p0}\delta\tau\right)}{\sin\left(\frac{1}{2}\omega_{p0}\delta\tau\right)}\right|. \quad (4)$$

Figure 3(b) shows the measured wake amplitude, as a function of pressure, for a pair of laser pulses. Very clear constructive and destructive interference of the two wakefields is observed, as expected. A fit to Eq. (4) yields $\delta\tau = (407 \pm 6)$ fs, which is in agreement with the values of (365 ± 40) and (420 ± 20) fs measured by the SSA and that deduced from interference fringes observed in the spectrum of the two drive pulses. Better agreement with the data is obtained if the pressure variation of the wake amplitude is calculated from the SSA measurement of the intensity profile of the driving pulses. For this fit the free parameters were an overall scaling factor for the wake amplitude, and a scaling factor α for the temporal axis of the measured driving pulses, such that $\zeta \to \alpha\zeta$; the fit yields $\alpha = 1.11 \pm 0.02$. An analysis of these data (see Supplemental Material [25]) shows that the second (smaller) laser pulse reduced the amplitude of the wakefield by $(44 \pm 8)\%$; this energy is removed from the plasma in the form of blue-shifted photons in the trailing laser pulse [32,33].

Figure 3(c) shows the measured wake amplitude as a function of the cell pressure for $N \approx 7$ laser pulses. A pronounced resonance is observed when the plasma period matches the pulse spacing $\delta\tau$. Also shown is a fit of Eq. (4) for a train of $N = 7$ identical pulses. Once again excellent agreement between the data and analytical theory is obtained, the fit yielding $\delta\tau = (116 \pm 2)$ fs, which agrees with the measured value. The solid line shows the variation of the wake amplitude calculated for the measured pulse train, the fit yielding $\alpha = 1.04 \pm 0.02$. It is noticeable that the pressure variation of the wake amplitude calculated for the measured pulse train does not exhibit subsidiary maxima; this difference is caused by the small variation of the pulse spacing, and the presence of temporal wings, in the measured pulse train.

We now place our results in context with earlier work. The MP-LWFA approach is closely related to the plasma beat-wave accelerator (PBWA) [1,34], in which two long laser pulses of angular frequencies ω_1 and $\omega_2 = \omega_1 + \omega_{p0}$ are combined to form a driving pulse modulated at ω_{p0}. Beat-wave excitation of plasma waves [35–37], and their application to accelerating electrons [38,39], have both been demonstrated.

A well-known problem with PBWA is that the relativistic increase in electron mass causes a loss of resonance between the wakefield and the driver, leading to saturation of the wake amplitude at the Rosenbluth-Liu limit [40]. A major advantage of MP-LWFA is that this limit can be overcome since the pulse spacing does not have to be constant within the train. Indeed, MP-LWFA can be considered to be a generalization of PBWA since, in addition, the properties of each pulse (i.e., the energy, wavelength, duration, etc.) can, in principle, be different. The MP-LWFA concept has been investigated theoretically [41–49] but has not previously been demonstrated experimentally. The idea of using a long pulse with temporally nonuniform modulation to overcome the Rosenbluth-Liu limit was proposed, within the context of PBWA, by Deutsch *et al.* [50], who suggested using a pair of frequency-chirped laser pulses.

Our results can be considered to be the first experimental demonstration of MP-LWFA or of beat-wave excitation with chirped laser pulses. In this first demonstration the pulse spacing within the train was approximately constant since the total available laser pulse energy was low; it would be straightforward to maintain resonant excitation with large amplitude wakefields by controlling the chirp of one or both pulses, for example, by an acousto-optic programmable filter [51]. Our results are important since they are the first experimental demonstration of wakefield excitation by a laser pulse structure that is long compared to the plasma period, and which has sufficient control to overcome relativistic saturation; as we have shown, this approach also offers the potential for energy recovery. The ability to deliver the driving laser energy over many plasma periods allows the use of high-repetition-rate laser systems, such as thin-disk [52] or fiber lasers [53], which cannot straightforwardly generate high-energy short laser pulses. These results, together with our earlier numerical analysis of this scheme [21], indicate a route to achieving highly controlled, GeV-scale laser-plasma accelerators operating at multikilohertz repetition rates and driven by novel, efficient laser technologies. In addition to stimulating new work on the development of laser-plasma accelerators, these results are of interest to those working on driving plasma accelerators driven by trains of particle bunches [54,55] or self-modulated proton beams [56,57].

This work was supported by the UK Science and Technology Facilities Council (STFC UK; Grant No. ST/J002011/1, ST/P002048/1, and 1507620); the Engineering and Physical Sciences Research Council (Grant Nos. 1378575 and 1093881); the Helmholtz Association of German Research centers (Grant No. VH-VI-503); and Effort sponsored by the Air Force Office of Scientific Research, Air Force Material Command, USAF, under Grant No. FA8655-13-1-2141. The U.S. Government is authorized to reproduce and distribute reprints for Governmental purpose notwithstanding any copyright notation thereon.

*simon.hooker@physics.ox.ac.uk

[1] T. Tajima and J. M. Dawson, Phys. Rev. Lett. **43**, 267 (1979).
[2] V. Malka, J. Faure, Y. A. Gauduel, E. Lefebvre, A. Rousse, and K. T. Phuoc, Nat. Phys. **4**, 447 (2008).
[3] E. Esarey, C. B. Schroeder, and W. P. Leemans, Rev. Mod. Phys. **81**, 1229 (2009).
[4] P. A. Norreys, Nat. Photonics **3**, 423 (2009).
[5] P. Chen, J. M. Dawson, R. W. Huff, and T. Katsouleas, Phys. Rev. Lett. **54**, 693 (1985).
[6] P. Muggli and M. J. Hogan, C.R. Phys. **10**, 116 (2009).
[7] S. M. Hooker, Nat. Photonics **7**, 775 (2013).
[8] W. P. Leemans, B. Nagler, A. J. Gonsalves, C. Toth, K. Nakamura, C. G. R. Geddes, E. Esarey, C. B. Schroeder, and S. M. Hooker, Nat. Phys. **2**, 696 (2006).
[9] S. Kneip *et al.*P. Rajeev, J. Schreiber, M. Streeter, D. Urner, J. Vieira, L. Silva, and Z. Najmudin, Phys. Rev. Lett. **103**, 035002 (2009).
[10] X. Wang *et al.*, Nat. Commun. **4**, 2988 (2013).
[11] A. Buck, M. Nicolai, K. Schmid, C. M. S. Sears, A. Sävert, J. M. Mikhailova, F. Krausz, M. C. Kaluza, and L. Veisz, Nat. Phys. **7**, 543 (2011).
[12] O. Lundh, J. Lim, C. Rechatin, L. Ammoura, A. Ben-Ismail, X. Davoine, G. Gallot, J.-P. Goddet, E. Lefebvre, V. Malka, and J. Faure, Nat. Phys. **7**, 219 (2011).
[13] M. Heigoldt, A. Popp, K. Khrennikov, J. Wenz, S.-W. Chou, S. Karsch, S. I. Bajlekov, S. M. Hooker, and B. Schmidt, Phys. Rev. ST Accel. Beams **18**, 121302 (2015).
[14] H.-P. Schlenvoigt, K. Haupt, A. Debus, F. Budde, O. Jackel, S. Pfotenhauer, H. Schwoerer, E. Rohwer, J. G. Gallacher, E. Brunetti, R. P. Shanks, S. M. Wiggins, and D. A. Jaroszynski, Nat. Phys. **4**, 130 (2008).
[15] M. Fuchs, R. Weingartner, A. Popp, Z. Major, S. Becker, J. Osterhoff, I. Cortrie, B. Zeitler, R. Hoerlein, G. D. Tsakiris, U. Schramm, T. P. Rowlands-Rees, S. M. Hooker, D. Habs, F. Krausz, S. Karsch, and F. Gruener, Nat. Phys. **5**, 826 (2009).
[16] S. Kneip *et al.*, Nat. Phys. **6**, 980 (2010).
[17] S. Cipiccia *et al.*, Nat. Phys. **7**, 867 (2011).
[18] K. T. Phuoc, S. Corde, C. Thaury, V. Malka, A. Tafzi, J.-P. Goddet, R. C. Shah, S. Sebban, and A. Rousse, Nat. Photonics **6**, 308 (2012).
[19] N. D. Powers, I. Ghebregziabher, G. Golovin, C. Liu, S. Chen, S. Banerjee, J. Zhang, and D. P. Umstadter, Nat. Photonics **8**, 28 (2013).
[20] K. Khrennikov, J. Wenz, A. Buck, J. Xu, M. Heigoldt, L. Veisz, and S. Karsch, Phys. Rev. Lett. **114**, 195003 (2015).
[21] S. M. Hooker, R. Bartolini, S. P. D. Mangles, A. Tuennermann, L. Corner, J. Limpert, A. Seryi, and R. Walczek, J. Phys. B **47**, 234003 (2014).
[22] C. Benedetti, C. B. Schroeder, E. Esarey, and W. P. Leemans, Phys. Plasmas **21**, 056706 (2014).
[23] A. Klenke, S. Hädrich, T. Eidam, J. Rothhardt, M. Kienel, S. Demmler, T. Gottschall, J. Limpert, and A. Tünnermann, Opt. Lett. **39**, 6875 (2014).
[24] N. H. Matlis, A. Maksimchuk, V. Yanovsky, W. P. Leemans, and M. C. Downer, Opt. Lett. **41**, 5503 (2016).
[25] See Supplemental Material http://link.aps.org/supplemental/10.1103/PhysRevLett.119.044802 for further details of the experimental arrangement and analysis methods.
[26] A. S. Weling and D. H. Auston, J. Opt. Soc. Am. B **13**, 2783 (1996).
[27] R. J. Shalloo, L. Corner, C. Arran, J. Cowley, G. Cheung, C. Thornton, R. walczak, and S. M. Hooker, Nucl. Instrum. Methods Phys. Res., Sect. A **829**, 383 (2016).
[28] N. H. Matlis, S. Reed, S. S. Bulanov, V. Chvykov, G. Kalintchenko, T. Matsuoka, P. Rousseau, V. Yanovsky, A. Maksimchuk, S. Kalmykov, G. Shvets, and M. C. Downer, Nat. Phys. **2**, 749 (2006).
[29] C. A. Arran, N. H. Matlis, L. Corner, J. Cowley, G. Cheung, C. D. Gregory, R. J. Shalloo, D. R. Symes, C. Thornton, R. Walczak, and S. M. Hooker (to be published).
[30] L. J. Spitzer, *Physics of Fully Ionized Gases* (John Wiley & Sons, New York, 1962).
[31] F. Dorchies, F. Amiranoff, V. Malka, J. R. Marques, A. Modena, D. Bernard, F. Jacquet, P. Mine, B. Cros, G. Matthieussent, P. Mora, A. Solodov, J. Morillo, and Z. Najmudin, Phys. Plasmas **6**, 2903 (1999).
[32] C. D. Murphy *et al.*, Phys. Plasmas **13**, 033108 (2006).
[33] J. M. Dias, L. OliveiraeSilva, and J. T. Mendonca, Phys. Rev. ST Accel. Beams **1**, 031301 (1998).
[34] C. Joshi, W. B. Mori, T. Katsouleas, J. M. Dawson, and J. M. Kindel, Nature (London) **311**, 525 (1984).
[35] A. E. Dangor, A. Dymoke-Bradshaw, and A. E. Dyson, Phys. Scr. **T30**, 107 (1990).
[36] C. E. Clayton, C. Joshi, C. B. C. Darrow, and D. Umstadter, Phys. Rev. Lett. **54**, 2343 (1985).
[37] F. Amiranoff, M. Laberge, J. R. Marques, F. Moulin, E. Fabre, B. Cros, G. Matthieussent, P. Benkheiri, F. Jacquet, J. Meyer, P. Mine, C. Stenz, and P. Mora, Phys. Rev. Lett. **68**, 3710 (1992).
[38] C. E. Clayton, K. A. Marsh, A. Dyson, M. Everett, A. LAL, W. P. Leemans, R. Williams, and C. Joshi, Phys. Rev. Lett. **70**, 37 (1993).
[39] S. Y. Tochitsky, R. Narang, C. V. Filip, P. Musumeci, C. E. Clayton, R. B. Yoder, K. A. Marsh, J. B. Rosenzweig, C. Pellegrini, and C. Joshi, Phys. Rev. Lett. **92**, 095004 (2004).
[40] M. N. Rosenbluth and C. S. Liu, Phys. Rev. Lett. **29**, 701 (1972).
[41] K. Nakajima, Phys. Rev. A **45**, 1149 (1992).
[42] V. I. Berezhiani and I. G. Murusidze, Phys. Scr. **45**, 87 (1992).
[43] D. Umstadter, E. Esarey, and J. Kim, Phys. Rev. Lett. **72**, 1224 (1994).

[44] D. A. Johnson, R. A. Cairns, R. Bingham, and U. De Angelis, Phys. Scr. **T52**, 77 (1994).
[45] S. Dalla and M. Lontano, Phys. Rev. E **49**, R1819 (1994).
[46] G. Bonnaud, D. Teychenné, and J.-L. Bobin, Phys. Rev. E **50**, R36 (1994).
[47] R. A. Cairns, D. Johnson, and R. Bingham, Laser Part. Beams **13**, 451 (1995).
[48] D. Umstadter, J. Kim, E. Esarey, E. Dodd, and T. Neubert, Phys. Rev. E **51**, 3484 (1995).
[49] E. I. Kalinnikova and V. D. Levchenko, Plasma Phys. Rep. **34**, 290 (2008).
[50] M. Deutsch, B. Meerson, and J. E. Golub, Phys. Fluids B **3**, 1773 (1991).
[51] F. Verluise, V. Laude, Z. Cheng, C. Spielmann, and P. Tournois, Opt. Lett. **25**, 575 (2000).
[52] T. Nubbemeyer, M. Kaumanns, M. Ueffing, M. Gorjan, A. Alismail, H. Fattahi, J. Brons, O. Pronin, H. G. Barros, Z. Major, T. Metzger, D. Sutter, and F. Krausz, Opt. Lett. **42**, 1381 (2017).
[53] C. Jauregui, J. Limpert, and A. Tünnermann, Nat. Photonics **7**, 861 (2013).
[54] P. Muggli, V. Yakimenko, M. Babzien, E. Kallos, and K. P. Kusche, Phys. Rev. Lett. **101**, 054801 (2008).
[55] E. Kallos, T. Katsouleas, W. D. Kimura, K. Kusche, P. Muggli, I. Pavlishin, I. Pogorelsky, D. Stolyarov, and V. Yakimenko, Phys. Rev. Lett. **100**, 074802 (2008).
[56] A. Caldwell, K. Lotov, A. Pukhov, and F. Simon, Nat. Phys. **5**, 363 (2009).
[57] A. Caldwell and K. V. Lotov, Phys. Plasmas **18**, 103101 (2011).